

# Impact of Gd dopants on current polarization and the resulting effect on spin transfer velocity in Permalloy wires

R. L. Thomas,<sup>1</sup> M. Zhu<sup>2,3,a)</sup> C. L. Dennis,<sup>4</sup> V. Misra,<sup>1</sup> and R. D. McMichael<sup>2</sup>

<sup>1</sup>*Department of Electrical & Computer Engineering North Carolina State University, Raleigh, NC, USA*

<sup>2</sup>*Center for Nanoscale Science and Technology, National Institute of Standards and Technology, Gaithersburg, Maryland 20899, USA*

<sup>3</sup>*Maryland Nanocenter, University of Maryland, College Park, Maryland 20742, USA*

<sup>4</sup>*Metallurgy Division, National Institute of Standards and Technology, Gaithersburg, Maryland 20899, USA*

A spin wave Doppler technique is used to measure the spin transfer velocity and the current polarization in current-carrying  $(\text{Ni}_{0.80}\text{Fe}_{0.20})_{1-x}\text{Gd}_x$  alloy wires. Reduced magnetization values with Gd doping suggest possible increases in the spin transfer velocity. Contrary to these expectations, we measured a decrease in the spin transfer velocity upon introducing Gd dopants. For a current density of  $10^{11}$  A/m<sup>2</sup>, the measured velocities range from 6.0 m/s  $\pm$  0.6 m/s for pure Permalloy ( $\text{Ni}_{0.80}\text{Fe}_{0.20}$ ) to 2.6 m/s  $\pm$  0.3 m/s for  $(\text{Ni}_{0.80}\text{Fe}_{0.20})_{0.945}\text{Gd}_{0.055}$ . Interpretation of these values yields a current polarization ranging from  $0.71 \pm 0.02$  to  $0.30 \pm 0.01$  for the same compositions. These results reveal that Gd dopants in Permalloy have a more significant impact on the current polarization than on the material's magnetization for these alloy compositions.

a) Current Address: Seagate Technology, Bloomington MN 55435

## I. INTRODUCTION

Magnetic domain wall devices based on propagating domain walls through ferromagnetic nanowires have been proposed for both memory<sup>1</sup> and logic applications.<sup>2</sup> The use of spin-polarized current to drive domain wall motion is a key aspect of these devices.<sup>3</sup> In order to develop these device concepts as viable technologies, the domain wall dynamics resulting from an applied current must be understood and optimized. However, the interactions between spin-polarized currents and domain walls are strongly dependent on material properties. Modulating the properties of magnetic materials and exploring the effect on dynamics provides further understanding and the potential to enhance the spin transfer torque effect.

The majority of research on domain wall devices has been performed using  $\text{Ni}_{0.80}\text{Fe}_{0.20}$  (Py, Permalloy) wires. However, current induced domain wall motion through Permalloy exhibits low domain wall velocities and requires high critical current densities to initiate motion.<sup>4-6</sup> It has been demonstrated that rare-earth dopants in Permalloy can be utilized to tune its magnetic properties, specifically the Gilbert damping constant, for applications such as magnetic storage technologies.<sup>7,8</sup> In this paper, we focus on the effect of Gd doping on the adiabatic spin transfer velocity,  $\mathbf{u}$ , in Permalloy.

The dynamics of the magnetization  $\mathbf{M}$  are described by the Landau-Lifshitz Gilbert (LLG) equation modified to include the influence of current,<sup>9,10</sup>

$$\frac{\partial \mathbf{M}}{\partial t} = \gamma \mu_0 \mathbf{H} \times \mathbf{M} + \frac{\alpha}{M_s} \mathbf{M} \times \frac{\partial \mathbf{M}}{\partial t} - (\mathbf{u} \cdot \nabla) \mathbf{M} + \frac{\beta}{M_s} \mathbf{M} \times [(\mathbf{u} \cdot \nabla) \mathbf{M}]. \quad (1)$$

The first and second terms on the right represent the precession and damping due to an effective magnetic field  $\mathbf{H}$  where  $\gamma$  is the gyromagnetic ratio and  $\alpha$  is the Gilbert damping factor. The last two terms, representing the adiabatic and nonadiabatic spin torques, account for the effects of a spin current. Here,  $\beta$  is the non-adiabatic factor and  $\mathbf{u}$  is the velocity caused by the adiabatic spin transfer torque. This term, also called the spin transfer velocity, is given by

$$\mathbf{u} = \frac{g \mu_B P}{2 M_s e} \mathbf{J} \quad (2)$$

where  $g$  is the Landé factor,  $\mu_B$  is the Bohr magneton,  $P$  is the current polarization,  $M_s$  is the saturation magnetization,  $e$  is the (negative) electron charge and  $\mathbf{J}$  is the current density.<sup>10</sup>

Since the operation speeds of domain wall devices are directly related to the domain wall velocities, faster propagation is desired for potential applications. In simple models, the current-driven domain wall velocity  $\mathbf{v}_{\text{DW}}$  below Walker breakdown is proportional to  $\mathbf{u}\beta/\alpha$ ,<sup>10,11</sup> and the critical current required to depin a domain wall is inversely proportional to this quantity.<sup>12</sup> Maximizing  $\mathbf{v}_{\text{DW}}$  requires a large value of  $\beta$ , a small value of  $\alpha$ , and as indicated by Eq. 2, low magnetization and large current polarizations. Because the spins of Permalloy and Gd atoms couple antiferromagnetically,<sup>13</sup> Gd doping can be used to reduce the net magnetization.<sup>7,8</sup> Furthermore, the Gd doping affects the damping only weakly.<sup>7,8</sup> However, the effect that Gd dopants have on polarization and  $\beta$  will determine the effectiveness of Gd doping in increasing  $\mathbf{v}_{\text{DW}}$ . Lepadatu et al. conclude from measurements of domain wall depinning that doping Permalloy with Gd increases the non-adiabatic factor  $\beta$  while inducing only small changes in the adiabatic spin transfer velocity,  $\mathbf{u}$ .<sup>14</sup> In this paper, we use the spin wave Doppler technique<sup>15-18</sup> to provide a direct measurement of the spin transfer velocity and the effect of Gd doping on the current polarization of Permalloy. Contrary to ref. 14, we find that Gd doping has a negative effect on both the current polarization and  $\mathbf{u}$ .

## II. EXPERIMENTAL DETAILS

A series of  $(\text{Ni}_{0.80}\text{Fe}_{0.20})_{1-x}\text{Gd}_x$  film compositions with Gd content varying from  $x = 0.0$  to  $x = 0.125$  were prepared via magnetron co-sputtering. Deposition rates were calibrated at various powers via profilometry and the RF power supplied to the Gd source was adjusted (at constant  $\text{Ni}_{0.80}\text{Fe}_{0.20}$  deposition power) to achieve various film compositions. Samples of unpatterned films were analyzed initially to determine the magnetic properties of these alloys. Both superconducting quantum interference device (SQUID) magnetometry and ferromagnetic resonance (FMR) measurements (described below) demonstrate the expected decrease in magnetization due to antiferromagnetic coupling between Permalloy and Gd atoms as shown in Fig. 1(a). The observed rate of magnetization decrease with Gd content is commensurate with previous results,<sup>7,8</sup> but Lepadatu et al. report a reduction in  $M$  that is an order of magnitude smaller.<sup>14</sup> In agreement with previous reports,<sup>7</sup> we measure an increase in film resistivity with Gd content (Fig. 1b) that is associated with the destruction of film crystallinity (Fig. 1c). Uncertainties in Fig. 1(b) are standard deviations associated primarily with uncertainty in thickness and width of device structures.

FMR spectra were taken using a coplanar waveguide with fixed frequencies from 2 GHz to 40 GHz and swept applied fields up to 1.2 T. The FMR results are summarized in Fig. 2. Values for effective magnetization  $M_{\text{eff}}$  and gyromagnetic ratio  $\gamma$  were determined by fitting the resonance field and frequency data to

$$f = \frac{\gamma\mu_0}{2\pi} [H_{\text{res}}(H_{\text{res}} + M_{\text{eff}})]^{1/2}. \quad (3)$$

The effective magnetization values are presented in Fig. 1.

SQUID magnetometry measures the magnetic moment of the film while FMR determines the effective magnetization characterizing the shape anisotropy of the film; differences can be attributed to perpendicular anisotropy. The damping parameters were determined by fitting line width measurements to

$$\Delta H = \Delta H_0 + \alpha \frac{4\pi f}{\sqrt{3}\gamma}. \quad (4)$$

The inhomogeneous broadening term  $\Delta H_0$  was less than 0.7 mT in each case, indicating high-quality, uniform films. Error bars in FMR data in Fig. 1(a) and Fig. 2(c,d) are standard deviations of the least-squares fits.

For Doppler measurements, the PyGd films were patterned using photolithography and lift-off techniques to obtain 30 nm thick wires with varying widths on high-resistivity Si wafers coated with a 20 nm  $\text{Al}_2\text{O}_3$  adhesion layer. Four DC contacts were patterned at the wire ends for current application and four-point resistance measurements. A 50 nm  $\text{Al}_2\text{O}_3$  insulating layer was evaporated prior to patterning microwave antennas over the wires via electron beam lithography. Other details concerning device fabrication are given elsewhere.<sup>16</sup> An example device used to obtain spin

wave Doppler measurements is shown in Fig. 3. The bulk magnetization of the wire is saturated by applying an in-plane static field perpendicular to the wire.

The microwave antennas, connected to the two ports of a vector network analyzer, emit and detect spin waves that propagate through the magnetic strip. The periodic structures of the antennas (inset of Fig. 3) couple primarily to the spin wave modes of two wave vectors:  $k_0 = 8.38 \mu\text{m}^{-1}$  and  $k_1 = 2.79 \mu\text{m}^{-1}$ . The transmission peaks due to these two wave vectors are well separated in frequency<sup>15,16</sup>. The transmission impedance values are extracted from the transmission coefficients measured from antenna to antenna and are averaged over 1,280 individual transmission spectra. The components due to spin waves are isolated by subtracting

background spectra at a reference field sufficient to shift the resonance outside the measured frequency window. Applying current to the magnetic wire shifts the spin wave angular frequency by an amount  $\Delta\omega = \mathbf{k} \cdot \mathbf{u}$  relative to the zero-current value.<sup>15</sup>

The high current densities applied during these measurements result in temperature increases due to Joule heating within the wire. Previous room temperature measurements of 4  $\mu\text{m}$  Permalloy wires indicated results from Doppler measurements were not compromised due to this heating because the spin transfer velocity in Permalloy is only weakly temperature dependent.<sup>16</sup> However, the effects of Joule heating become more pronounced in film compositions with higher Gd content due to increased resistivity.

The effect of heating in wires of various widths was analyzed by measuring resistance as a function of temperature on a heated chuck. The changes in resistance due to high current density were then measured. In 8  $\mu\text{m}$  wires with 8 % Gd content, the maximum current density of  $1.2 \times 10^{11} \text{ A/m}^2$  caused the resistance to increase by a fraction of 10 % while in 2  $\mu\text{m}$  wires the fractional increase in resistance was only 2.5 %. By correlating these values with our temperature dependent resistance measurements, we estimate temperature changes of 136 K and 34 K respectively. We conclude that wider wires exhibit a greater temperature increase than more narrow wires because they require larger currents to accomplish the same current density. To avoid issues with heating, the results shown in this paper are limited to 2  $\mu\text{m}$  wires. In the measurements, we ensure that variations in Joule heating are kept to a minimum by holding the current constant while measuring the transmission of spin waves parallel and antiparallel to the current direction. Consequently, the frequency shifts measured are caused by the applied current rather than temperature variations and their magnitudes are twice as large (from  $-J$  to  $+J$ ) as theoretical shifts occurring with and without current flowing through the device (from 0 to  $\pm J$ ).

### III. EXPERIMENTAL RESULTS

An example of the frequency shifts that occur between transmission impedances,  $Z_{12}$  and  $Z_{21}$ , is shown in Fig. 4(a) for a  $\text{Py}_{0.96}\text{Gd}_{0.04}$  wire. In the upper panel, a positive current density of  $1.3 \times 10^{11} \text{ A/m}^2$  is applied to the wire shifting  $Z_{12}$  and  $Z_{21}$  to higher and lower frequencies respectively. Reversing the current also reverses the sign of the frequency shift as shown in the lower panel. The frequency shift is estimated over the displayed range in Fig. 4(a) and found by fitting the autocorrelation function of the transmission spectra to locate the maximum. Standard errors in the frequency shift were less than 0.070 MHz for all such fits. However, the frequency shift is dependent on the range of values selected for each fit. As a result, we conservatively estimate our maximum uncertainty as the minimum frequency step size of the spectrum if 2.5 MHz.

The current-dependent frequency shift,  $\Delta f$ , for samples with different Gd content are shown in Fig. 4(b). The spin transfer velocity is obtained from the frequency shift where  $u = \pi\Delta f/k$ . Spin transfer velocities for a current density of  $10^{11} \text{ A/m}^2$  were extracted from the slopes of the linear fits for varying Gd content and plotted in Fig. 4(c).

Error bars are the combined uncertainties from uncertainty in width and thickness of the stripe, uncertainty in wavelength of spin waves and standard deviation of the linear fit. We verified the measurements by comparing multiple devices for each concentration, and the spin transfer velocity measurements were within the error bars on all compositions except the  $\text{Py}_{0.92}\text{Gd}_{0.08}$  samples. Four different  $\text{Py}_{0.92}\text{Gd}_{0.08}$  device samples were measured yielding a range from  $(3.7 \pm 0.4) \text{ m/s}$  to  $(5.4 \pm 0.6) \text{ m/s}$ . We speculate that these highly doped amorphous films show greater variation because changes can occur in the microstructure of these films due to

the heating at large current densities applied during measurements. An average velocity of  $(4.3 \pm 0.5)$  m/s was obtained by applying a linear fit to all the acquired data points at the current density of  $10^{11}$  A/m<sup>2</sup>. The minimum value for the spin transfer velocity is  $(2.6 \pm 0.3)$  m/s for 5.5 % Gd content. This is a fractional reduction of 57 % from the value for Permalloy,  $(6.0 \pm 0.6)$  m/s. Introducing Gd dopants results in a reduction of the spin transfer velocity, an effect that contradicts expectations based solely on the decrease in magnetization.

Using the spin transfer velocity equation (2), polarization values are extracted using the slope of  $\mathbf{u}$  vs.  $\mathbf{J}$  and the magnetization data obtained by SQUID measurements. As expected, the polarization values as a function of Gd dopant content follow the trend of the spin transfer velocity, also reaching a minimum at the  $\text{Py}_{0.945}\text{Gd}_{0.055}$  composition as shown in Fig. 5(a).

The spin-up and spin-down conductivities of these alloys are obtained using:  $\sigma_{\uparrow} = (1+P)/2\rho$  and  $\sigma_{\downarrow} = (1-P)/2\rho$ . These quantities are plotted in Fig. 5(b). In agreement with the previous results for Permalloy, we find the spin-up conductivity to be much larger than the spin-down conductivity.<sup>16</sup> The spin-up conductivity shows a monotonic decrease with the largest effect occurring between samples consisting of 4 % and 5.5 % Gd content. The spin down conductivity shows an initial increase but decreases for concentrations above 4 % Gd content. The simultaneous increase in the minority conductivity and decrease in the majority conductivity is an effect expected for increased spin flip scattering.<sup>16,19</sup> Spin flip scattering mixes the majority and minority conduction channels, reducing the polarization.

#### IV. DISCUSSION

We finish with speculation on the prospects for increasing the current driven domain wall velocity via further Gd doping of Permalloy. The relative increase in both spin transfer velocity and polarization between the  $\text{Py}_{0.945}\text{Gd}_{0.055}$  and the  $\text{Py}_{0.92}\text{Gd}_{0.08}$  compositions (Fig. 4c) suggests that the spin transfer velocity may increase with further Gd doping. Unfortunately, due to its low magnetization and increased damping value, the alloy with  $x = 0.10$  Gd content did not provide sufficient spin wave transmission signal to allow spin transfer velocity measurements.

In conclusion, we have measured the spin transfer velocity and polarization in PyGd wires using the spin wave Doppler technique. The current polarization of  $(\text{Ni}_{0.80}\text{Fe}_{0.20})_{1-x}\text{Gd}_x$  decreases for compositions with up to  $x = 0.055$  Gd content, corresponding to an overall decrease in spin transfer velocity. Compositions with higher Gd content demonstrate the potential to possess larger current polarizations and spin transfer velocities. We conclude that modulating the properties of Permalloy by introducing Gd dopants has a strong impact on the material's current polarization.

#### V. ACKNOWLEDGEMENTS

We are grateful for the assistance of the Center for Nanoscale Science and Technology (CNST) Nanofab staff, especially Richard Kasica on electron-beam lithography and to John Read for preliminary FMR measurements. This work has been supported in part by the NIST-CNST/UMD-Nanocenter Cooperative Agreement, the Semiconductor Research Corporation and the U.S. Department of Education's Graduate Assistance in Areas on National Need (GAANN) program.

<sup>1</sup>S. S. P. Parkin, M. Hayashi, and L. Thomas, *Science* **320**, 190 (2008).

<sup>2</sup>D. A. Allwood, G. Xiong, C. C. Faulkner, D. Atkinson, D. Petit, and R. P. Cowburn, *Science* **309**, 1688 (2005).

<sup>3</sup>L. Berger, *Journal of Applied Physics* **55**, 1954 (1984).

<sup>4</sup>M. Hayashi, L. Thomas, R. Moriya, C. Rettner, and S. S. P. Parkin, *Science* **320**, 209 (2008).

<sup>5</sup>M. Klaui, M. Laufenberg, L. Heyne, D. Backes, U. Rudiger, C. A. F. Vaz, J. A. C. Bland, L. J. Heyderman, S. Cherifi, A. Locatelli, T. O. Mentis, and L. Aballe, *Applied Physics Letters* **88**, 232507 (2006).

<sup>6</sup>A. Yamaguchi, T. Ono, S. Nasu, K. Miyake, K. Mibu, and T. Shinjo, *Physical Review Letters* **92**, 077205 (2004).

<sup>7</sup>W. Bailey, P. Kabos, F. Mancoff, and S. Russek, *Ieee Transactions on Magnetics* **37**, 1749 (2001).

<sup>8</sup>G. Woltersdorf, M. Kiessling, G. Meyer, J. U. Thiele, and C. H. Back, *Physical Review Letters* **102**, 257602 (2009).

<sup>9</sup>S. Zhang and Z. Li, *Physical Review Letters* **93**, 127204 (2004).

<sup>10</sup>A. Thiaville, Y. Nakatani, J. Miltat, and Y. Suzuki, *Europhysics Letters* **69**, 990 (2005).

- <sup>11</sup>T. A. Moore, M. Klaui, L. Heyne, P. Mohrke, D. Backes, J. Rhensius, U. Rudiger, L. J. Heyderman, J. U. Thiele, G. Woltersdorf, C. H. Back, A. F. Rodriguez, F. Nolting, T. O. Montes, M. A. Nino, A. Locatelli, A. Potenza, H. Marchetto, S. Cavill, and S. S. Dhesi, *Physical Review B* **80**, 132403 (2009).
- <sup>12</sup>G. S. D. Beach, M. Tsoi, and J. L. Erskine, *Journal of Magnetism and Magnetic Materials* **320**, 1272 (2008).
- <sup>13</sup>K. N. R. Taylor, *Advances in Physics* **20**, 551 (1971).
- <sup>14</sup>S. Lepadatu, J. Claydon, D. Ciudad, A. Naylor, C. Kinane, S. Langridge, S. Dhesi, and C. Marrows, *Applied Physics Express* **3**, 083002 (2010).
- <sup>15</sup>V. Vlaminc and M. Bailleul, *Science* **322**, 410 (2008).
- <sup>16</sup>M. Zhu, C. L. Dennis, and R. D. McMichael, *Physical Review B* **81**, 140407 (2010).
- <sup>17</sup>V. Vlaminc and M. Bailleul, *Physical Review B* **81**, 014425 (2010).
- <sup>18</sup>M. Zhu, B. D. Soe, R. D. McMichael, M. J. Carey, S. Maat, and J. R. Childress, *Applied Physics Letters* **98**, 083002 (2010).
- <sup>19</sup>A. Fert and I. A. Campbell, *Journal of Physics F-Metal Physics* **6**, 849 (1976).

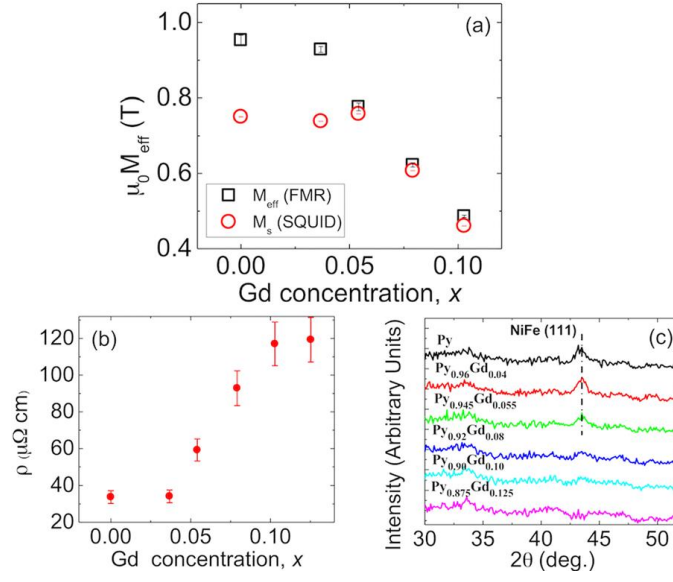


FIG. 1: (Color online) (a) Magnetization and (b) resistivity as a function of Gd concentration. (c) X-ray diffraction measurements of the NiFe (111) peak for PyGd alloys showing transformation from crystalline to amorphous films complete at 8 % Gd concentration.

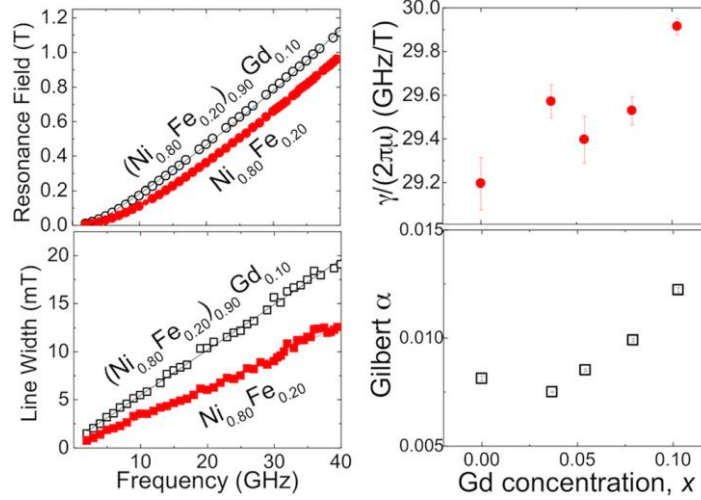


FIG. 2: (Color online) (a) Ferromagnetic resonance field and (b) line width as a function of excitation frequency for two representative samples. The small line width values obtained by extrapolation to zero frequency are indicative of high uniformity films. (c) Fitting of the resonance fields yields the gyromagnetic ratio and (d) fitting of the line width yields the damping parameter.

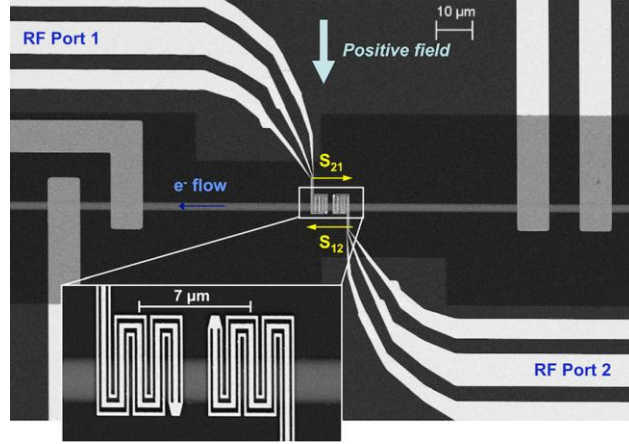


FIG. 3: (Color online) Scanning electron microscope (SEM) image of the fabricated Doppler device with a 2  $\mu\text{m}$  wide PyGd wire, seen here as a thin horizontal line.  $S_{12}$  ( $S_{21}$ ) refers to the spin wave transmission from RF port 2(1) to port 1(2). The direction of electron flow for positive current is represented by the arrow in the image. The inset shows a magnified image of the microwave antennas with a center-to-center distance of 7  $\mu\text{m}$ .

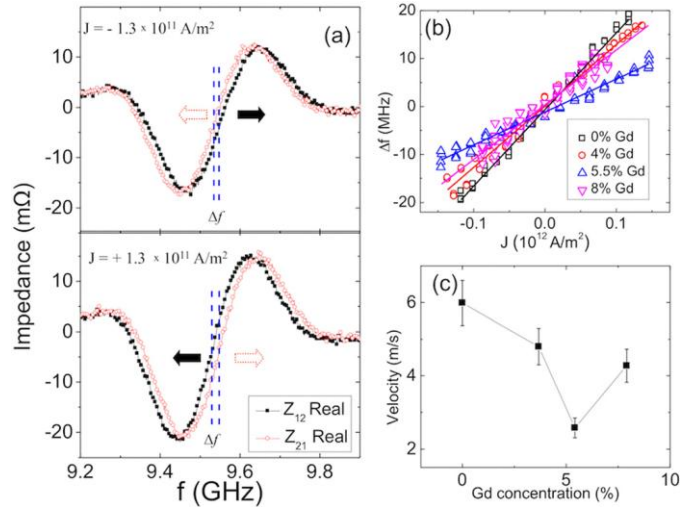


FIG. 4: (Color online) (a) Real part of the transmission impedance  $Z_{12}$  and  $Z_{21}$  when a current density of  $\pm 1.3 \times 10^{11} \text{ A/m}^2$  flows through the  $\text{Py}_{0.90}\text{Gd}_{0.10}$  wire. (b) The relative frequency shift,  $\Delta f$ , as a function of applied current density for different PyGd alloys with linear fits. (c) Spin transfer velocity as a function of Gd concentration for a current density of  $10^{11} \text{ A/m}^2$ .

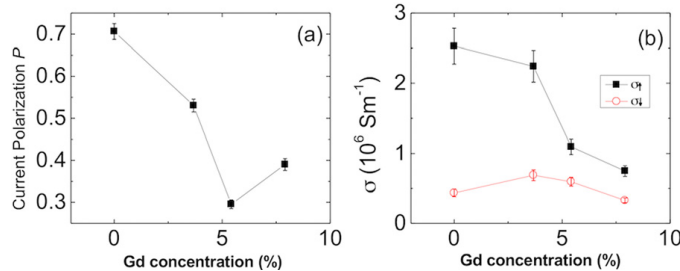


FIG. 5: (a) Current polarization of PyGd alloys. (b) Spin-up and spin-down conductivities as a function of Gd concentration.